ARCHIVES OF ELECTRICAL ENGINEERING VOL. 68(3), pp. 521–533 (2019)

DOI 10.24425/aee.2019.129339

Influence of multi-tine electrode configuration in realistic hepatic RF ablative heating

PIOTR GAS[1], JOANNA WYSZKOWSKA[2]

[1] *AGH University of Science and Technology*
Department of Electrical and Power Engineering
al. Mickiewicza 30, 30-059 Krakow, Poland

[2] *Nicolaus Copernicus University*
Faculty of Biology and Environmental Protection
Lwowska 1, 87-100 Torun, Poland
e-mails: piotr.gas@agh.edu.pl, joanna.wyszkowska@umk.pl

(Received: 18.12.2018, revised: 13.03.2019)

Abstract: Percutaneous RF ablation is one of alternative treatment for non-surgical liver tumors. Ablative changes in hepatic tissue can be successfully estimated using the finite element method. The authors created a 3D model of a multi-tine applicator immersed in liver tissue, and then determined the optimal values of voltage applied to such an RF electrode, which do not exceed the therapeutic temperature range valid during thermal ablation procedure. Importantly, the simulations were carried out for the RF electric probes with 2 to 5 evenly spaced arms. Additionally, the thermal damage of hepatic tissue for multi-armed applicators working at pre-defined limit values of voltages was established based on the Arrhenius model.

Key words: percutaneous RF ablation, multi-tine electrode, tumor heating techniques, Arrhenius thermal damaged model, hepatocellular carcinoma, finite element method

1. Introduction

Hepatocellular carcinoma is the most common malignant tumor located in the human liver, affecting an increasing number of general population [1]. However, in most cases, hepatic malignances cannot be cured by surgical resection [2]. This is mainly due to the size and structure of multifocal liver tumor, its location and dense vascularity. For this reason, others innovative and minimally invasive heating techniques that save large volumes of tissue and focus heat in the

selected volume of the body, are wanted to be found [3, 4]. The examples of focal thermotherapies are the so-called interstitial hyperthermia and thermal ablation [5, 6] which both use RF energy [7] or microwaves [8]. Importantly, the interstitial techniques, due to simple construction and usage of a thin, needle applicator [9], do not require laparotomy and may be applied percutaneously during general anesthesia [10]. The commonly used probes for thermal therapies can be temperature- or power-controlled [2] and often aided with thermal sensors and various image-guided techniques [11]. The tissue temperature during ablation can reach significant values ranging from 50°C to 110°C [3], that combined with right application time may ultimately lead to coagulation and tissue necrosis [5, 12–14]. It should be noticed, that burning of tumors takes place with a certain margin of ablative tissue necrosis, difficult to unambiguously determine using available imaging methods during ablation procedures. It creates the possibility of thermal damage to adjacent nerves, blood vessels and surrounding tissues and limits the usage of this method [15]. Moreover, the inadequate shape of the applicator, its location and used power (temperature) can contribute to incomplete destruction of cancer cells and cause recurrence of neoplastic disease.

Based on the paper [2], the authors created a 3D model of a multi-tine probe immersed inside liver tissue, and then established the optimal values of the voltage applied to the utilized RF electrode, that do not exceed therapeutic levels of temperature during thermal ablation. Thus, temperature at the tip of the main tine-probe was treated as a control parameter. The simulations were carried out for an RF electrode with 2–5 regularly spaced arms. Next, the thermal damage of hepatic tissue for the multi-tine applicator and pre-defined limit values of electrode voltage was specified based on the Arrhenius model. Similar considerations can be found in several related papers concerning different kind of electric probes [16–27].

2. Model definition and governing equations

The model of multi-tine electric probe is shown in Fig. 1. This applicator, designed specially for tissue thermal ablation, consists of a cylindrical stainless steel trocar and several half-torus-shaped nickel-titanium tines. The upper part of the trocar (called trocar tip) and the arms coming out from the trocar tip (called tines of electrode) form a conductive RF electrode, where the electric voltage V_0 is applied. Importantly, the trocar is powered from a 50-ohm feeding line. All electric probe dimensions (see Fig. 1) were adopted from [2] and summarized in Table 1. Importantly, the RF applicator was analyzed in a rectangular coordinate system (x, y, z) inside a computational area with dimensions 10 cm × 10 cm × 12 cm.

For simplicity, the presented 3D model of RF heating of liver tissue assumes a quasi-static approximation for an electro-conductive field based on the following equations [16]:

$$\nabla \cdot \boldsymbol{J} = 0, \tag{1}$$

$$\boldsymbol{J} = \sigma \boldsymbol{E}, \tag{2}$$

$$\boldsymbol{E} = -\nabla \varphi, \tag{3}$$

where $\boldsymbol{J}$ (A/m^2) and $\boldsymbol{E}$ (V/m) stand for the vectors of current density and electric field intensity, respectively. Moreover, σ (S/m) means the electric conductivity of a given medium and φ (V) is the electric potential.

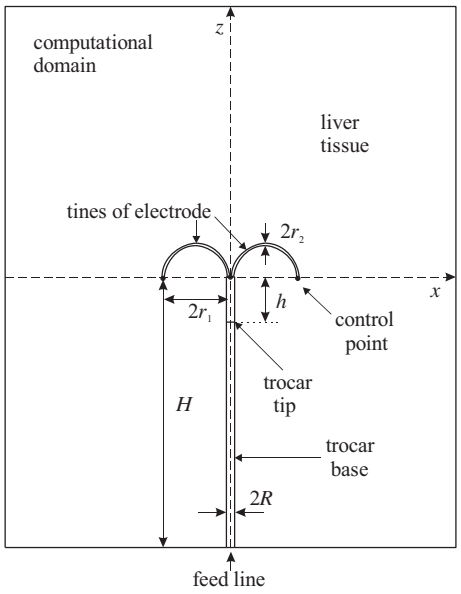

Fig. 1. Geometrical model of a 3D applicator for RF ablation in the *xz*-plane

Table 1. Geometrical dimensions of the RF probe [2]

Applicator elements	**Size** (mm)
radius of the trocar	$R = 0.9144$
outer radius of the electrode	$r_1 = 7.5000$
inner radius of the electrode	$r_2 = 0.2667$
length of the trocar	$H = 60$
length of the trocar tip	$H = 10$

Such an assumption is true for the RF range of 450–550 kHz, where the wavelength of the EM excitation ($\lambda = c_0/f \approx 600$ m) is much larger than the dimensions of the analyzed geometry (about 10 000 times more than the largest applicator size, see Table 1) [16]. Therefore, the displacement currents are negligibly compared to the conduction currents [12]. It was assumed that all the modelled materials are considered as isotropic, homogeneous and linear media. Because the electric field distribution within a computational area is forced by the electric potential applied on the RF electrode the Laplace equation should be employed to solve the described problem [24, 25, 27]:

$$\nabla \cdot (-\sigma \nabla \varphi) = 0. \tag{4}$$

The temperature distribution within the hepatic tissue under RF heating can be estimated from the bioheat transfer Pennes equation [28]:

$$\rho C \frac{\partial T}{\partial t} + \nabla \cdot (-\kappa \nabla T) = \rho_b C_b \omega_b (T_b - T) + Q_{ext} + Q_{met}\,, \tag{5}$$

where ρ, C, and κ mean the mass density (kg/m^3), the specific heat (J/(kg·K)), and the thermal conductivity of a given material (W/(m·K)), respectively, T is the unknown temperature (K), and t is the time (s). Importantly, the blood parameters are provided with subscript 'b', as in the case of ω_b (1/s), which means the blood perfusion rate in liver tissue. Moreover, the term Q_{ext} (W/m^3) denotes the Joule heating [12, 16, 18, 26]:

$$Q_{ext} = \boldsymbol{J} \cdot \boldsymbol{E} = \sigma |\boldsymbol{E}|^2 = \sigma \, |\nabla \varphi|^2 , \tag{6}$$

where $|\boldsymbol{E}|$ (V/m) means a modulus of electric field strength. In addition, Q_{met} (W/m^3) is the volumetric heat generated due to hepatic tissue metabolism. What is important, the heat flow within the multi-tine electric probe is analyzed by omitting the term related to blood perfusion.

To solve such a coupled problem, initial and boundary conditions for basic Equations (4) and (5) should be given. An initial voltage has a zero value ($\varphi_0 = 0$). The electric insulation ($\partial\varphi/\partial n = 0$) was assumed on the outer boundaries of the computational area. Moreover, the electric potential/voltage ($\varphi = V_0$) was applied on the electrode surface, namely tines of the electrode and the trocar tip (see Fig. 1). For other surfaces, the continuity of the normal components of the current density vector was assumed, according to the formula:

$$\boldsymbol{n} \cdot (\boldsymbol{J}_1 - \boldsymbol{J}_2) = 0, \tag{7}$$

with the following equivalent form:

$$\boldsymbol{n} \cdot (\sigma_1 \nabla \varphi_1 - \sigma_2 \nabla \varphi_2) = 0. \tag{8}$$

In addition, the initial temperature for all the domains is equal to T_0. All the external boundaries characterize temperature $T = T_b$. Besides, the continuity of heat flow within all the interior boundaries was assumed using the condition:

$$\boldsymbol{n} \cdot (\kappa_1 \nabla T_1 - \kappa_2 \nabla T_2) = 0, \tag{9}$$

where $\boldsymbol{n}$ is the unit vector normal to given surface. Importantly, the physical quantities marked by subscripts 1 and 2 correspond to their values in two different sides of a given boundary.

2.1. Arrhenius thermal damage model of tissue

A model of tissue thermal damage following ablation treatment can be derived from the chemical kinetics and collision theory based on a single-step-type chemical reaction [5]:

$$\beta \mathrm{A} \rightarrow \gamma \mathrm{B}, \tag{10}$$

which transforms substance A (also called reagent or substrate) into substance B (product) with proper stoichiometric coefficients, β and γ. Such a chemical reaction proceeds with a specific reaction rate r outlined by the ordinary differential equations system, namely [29]:

$$r = -\frac{1}{\beta} \frac{\mathrm{d}[\mathrm{A}]}{\mathrm{d}t} = \frac{1}{\gamma} \frac{\mathrm{d}[\mathrm{B}]}{\mathrm{d}t}, \tag{11}$$

where $[\mathrm{A}] = n_\mathrm{A}/V$ and $[\mathrm{B}] = n_\mathrm{B}/V$ (mol/L) stand for the molar concentrations, n_A and n_B (mol) mean the mole numbers of ingredients A and B, respectively, and V (m^3) indicates the mixture

volume. It is worth noting that any mole of substance A contains $N_{\mathrm{A}} = 6.022140857 \cdot 10^{23}$ molecules of substance A, where N_{A} is the so-called Avogadro number. Moreover, with the growing reagent concentrations, the reaction rate, related to the probability of particle collisions, also increases, which is described by the following rate law [30]:

$$r = k(T)\,[\mathrm{A}]^{\beta}\,[\mathrm{B}]^{\gamma}, \tag{12}$$

where $k(T)$ represents a temperature-dependent reaction rate constant usually expressed with units (L/mol/s) or (1/s) depending on the order of the analyzed chemical reaction.

What is important, the particle collisions themselves are not enough for the reaction (10) to occur. The colliding molecules of substance A should interact with each other with a proper level of the activation energy E_{a} to overcome the energetic barriers specified for a given type of chemical reaction. Since particles are different in terms of their dimensions and speed of collisions, they interact with various activation energies, and therefore the statistical thermodynamics and in particular the Maxwell-Boltzmann distribution should be employed in the current model. Using the so-called collision theory, the proportionality constant for the above equation can be determined from the well-known Arrhenius relation [5]:

$$k(T) = A \exp\left(-\frac{E_{\mathrm{a}}}{E_T}\right) = A \exp\left(-\frac{E_{\mathrm{a}}}{\mathrm{R}T}\right), \tag{13}$$

where A is the so-called frequency factor (1/s), E_{a} and E_T mean the activation energy (J/mol) and the averaged thermal energy (J/mol) of colliding particles, respectively, What is more, $\mathrm{R} = 8.3144598$ J/(mol K) indicates an universal gas constant. It should be emphasized that the Arrhenius model assumes all particles are in a state of thermodynamic equilibrium and interact with each other only through elastic collisions with a specified frequency A, similarly to molecules of ideal gas.

In the case of thermotherapies like ablation treatments, the tissue thermal damage may be simplified to the two-state denaturation process governed by chemical reaction of the first order. Ablation leads to the irreversible destruction of living cells (L), under the influence of high temperature, causing them necrosis, death and formation of dead cells (D) [12, 29]:

$$\mathrm{L} \xrightarrow{T,\,E_{\mathrm{a}}} \mathrm{D}. \tag{14}$$

According to (11)–(13), the reaction rate may be rewritten in the following form [5]:

$$r = -\frac{\mathrm{d}[\mathrm{L}]}{\mathrm{d}t} = k(T)[\mathrm{L}] = A \exp\left(-\frac{E_{\mathrm{a}}}{\mathrm{R}T}\right)[\mathrm{L}], \tag{15}$$

where $k(T)$ is the overall temperature denaturation rate, which depends on both the activation energy E_{a} and the temperature T of the described process.

In the next step, after substituting the concentration of living cells [L] into an equivalent function $c(\boldsymbol{r}, t)$ dependent on the position vector $\boldsymbol{r} = (x,\, y,\, z)$ and time t, we yield:

$$\frac{\partial c(\boldsymbol{r}, t)}{\partial t} = -A \exp\left(-\frac{E_{\mathrm{a}}}{\mathrm{R}T(\boldsymbol{r}, t)}\right) c(\boldsymbol{r}, t), \tag{16}$$

which, after dividing by the function $c(\boldsymbol{r},t)$, results in:

$$\frac{\partial \ln c(\boldsymbol{r},t)}{\partial t} = -A\exp\left(-\frac{E_\mathrm{a}}{\mathrm{R}T(\boldsymbol{r},t)}\right). \tag{17}$$

The so-called tissue damage rate is defined by [14]:

$$\frac{\partial \Omega(\boldsymbol{r},t)}{\partial t} = -\frac{\partial \ln c(\boldsymbol{r},t)}{\partial t} A\exp\left(-\frac{E_\mathrm{a}}{\mathrm{R}T(\boldsymbol{r},t)}\right) = k(T). \tag{18}$$

Finally, by integrating (18) over time, we obtain the so-called Arrhenius damage index or simply the Arrhenius integral, which specifies the total injury degree of tissue [12, 19, 22, 25]:

$$\Omega(\boldsymbol{r},t) = \ln\left[\frac{c(\boldsymbol{r},0)}{c(\boldsymbol{r},t)}\right] = A\int_0^t \exp\left(-\frac{-E_\mathrm{a}}{\mathrm{R}T(\boldsymbol{r},\tau)}\right)\mathrm{d}\tau = \int_0^t k(T)\,\mathrm{d}\tau. \tag{19}$$

Initially, before the ablation procedure, the Ω-parameter has a zero value, but during the therapy, the Arrhenius integral value rises linearly in time or hyperbolically with temperature. It is worth noting that for $\Omega = 1$ and $\Omega = 4.63$ the probability of permanent cell destruction is, respectively, at a level of 63% and 99% [5, 7, 18, 25].

In addition, the survival and necrotic fractions of the tissue can be predicted respectively from the relations as follows [5, 14]:

$$\alpha(\boldsymbol{r},t) = \frac{c(\boldsymbol{r},t)}{c(\boldsymbol{r},0)}\exp\left[-\Omega(\boldsymbol{r},t)\right], \tag{20}$$

$$\theta(\boldsymbol{r},t) = 1-\alpha(\boldsymbol{r},t) = 1-\exp\left[-\Omega(\boldsymbol{r},t)\right]. \tag{21}$$

The α-parameter specifies the probability of cells survival and varies from 1 at the initial time (where all tissue cells are alive) to 0 after a certain time of treatment (where all living cells are destroyed). On the other hand, the θ-coefficient changes its values from 0 to 1 and is related to the probability of thermal damage of treated cells which may be essential in cancer therapy.

3. Calculation results

The current model assumes a quasi-static approximation and is valid for a frequency of $f = 500$ kHz. The parameters used for modelling hepatic tissue, blood and an RF applicator have been taken from the paper [2] and listed in Table 2. Furthermore, the model assumes blood perfusion through liver tissue with a rate of $\omega_\mathrm{b} = 6.4\cdot 10^{-3}$ 1/s and omits the metabolic heat generation ($Q_\mathrm{met} = 0$). In addition, $T_0 = T_\mathrm{b} = 37°\mathrm{C}$ and parameters of the Arrhenius model for hepatic tissue were accepted as $A = 7.39\cdot 10^{39}$ 1/s and $E_\mathrm{a} = 2.577\cdot 10^5$ J/mol [5, 7].

All the presented below calculations are based on the finite element method and have been carried out in Comsol Multiphysics software. All the analyzed RF probes with evenly distributed tines are compared together in Fig. 2. The simulation showed that the electrode potential employed

Table 2. Fitting parameters for used electro-thermal model [2]

Modelled elements	σ (S/m)	ρ (kg/m^3)	C (J/(kg·K))	κ (W/(m·K))
electrode	10^8	6 450	840	18
trocar tip	$4 \cdot 10^6$	21 500	132	71
trocar base	10^{-5}	70	45	0.026
liver tissue	0.333	1079	3540	0.520
blood	0.667	1000	4180	0.543

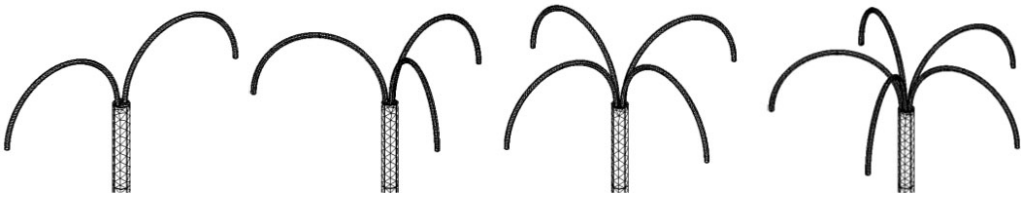

(a) (b) (c) (d)

Fig. 2. Division of RF applicators into finite elements in analyzed cases of multi-tine electrodes with: (a) 2; (b) 3; (c) 4; (d) 5 evenly distributed arms

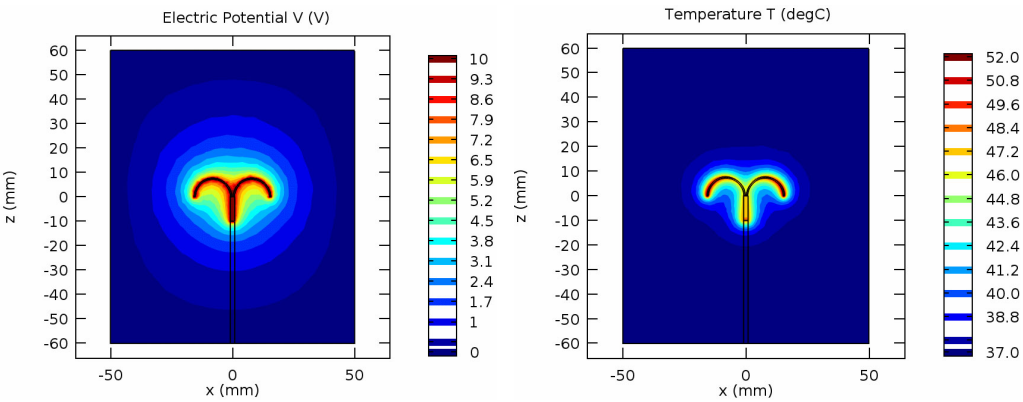

(a) (b)

Fig. 3. Examples of *xz*-distributions of: (a) electric potential, and (b) temperature within human liver during ablation heating for the 2-tine electrode at voltage $V_0 = 10$ V

directly affects the temperature inside a volume of interest. Fig. 3 illustrates contour plots of electric potential and temperature distributions in the *xz*-plane for the exemplary voltage ($V_0 = 10$ V) applied to the 2-tines electrode.

In the first step of the optimization approach, the limits of employed voltage were specified for therapeutic levels of temperature valid in ablation procedure (50°C–110°C). This was done in

a simple way by parametrically changing of the employed voltage and observation of the values of temperature in the control points at the electrode-tissue interface (Fig. 4(a)). It turned out that the temperature at the opposite tips of the two-armed probe is practically the same (and slightly higher than the temperature in the origin), which results from the geometrical symmetry of the employed RF applicator. Therefore, the point (15.5, 0, 0) of the first tip of the multi-tine electrode was chosen for later observations. In the next step, the temperature was determined for the predefined optimal voltage values of the 2-tine electrode, thus checking the temperature at the control point does not exceed the therapeutic levels (Fig. 4(b)). A similar procedure was conducted for electrodes with 3, 4 and 5 arms. Table 3 compares the limit values of the voltage applied to various multi-tine electrodes. It should be emphasized that N tines of such an electric probe are evenly distributed, and an angle ϕ between them is observed in the xy-plane. Importantly, the condition $N \cdot \phi = 360^\circ$ is fulfilled in any analyzed case. Interestingly, the growing number of electrode tines requires constant increase of electrode voltage, to maintain the same temperature levels.

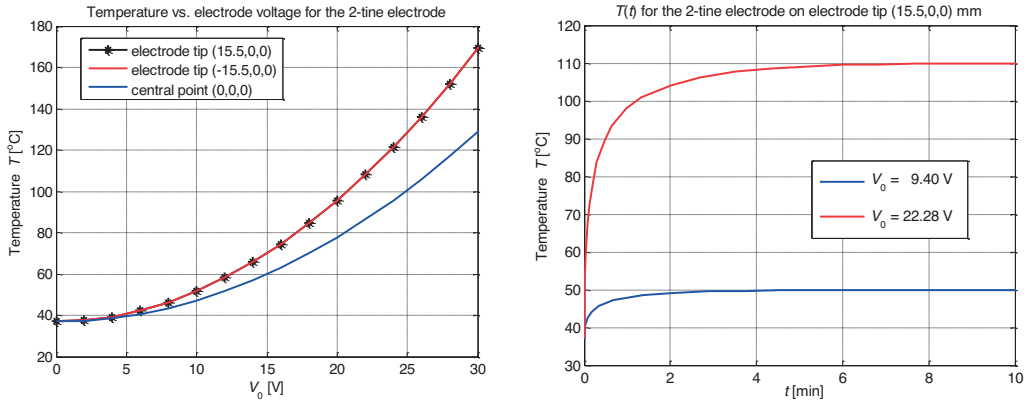

(a) (b)

Fig. 4. Distributions of: (a) temperature versus electrode voltage for different control points of the 2-tine electrode and (b) temperature versus time on tip of the 2-tine electrode for established limit values of applied voltage within hepatic tissue during ablation treatment

Table 3. Voltages applied to the multi-tine electrodes

Limit values of electrode voltage	**2-tine electrode** ($\phi = 180^\circ$)	**3-tine electrode** ($\phi = 120^\circ$)	**4-tine electrode** ($\phi = 90^\circ$)	**5-tine electrode** ($\phi = 72^\circ$)
$V_{0\,\min}$ (V)	9.40	9.78	10.19	10.58
$V_{0\,\max}$ (V)	22.28	23.18	24.14	25.08

The next Fig. 5 presents isotherms for temperature 50°C in the xy-plane for all analyzed multi-tine electrodes during ablation treatment with the maximum allowed temperature 110°C, which corresponds to the employed voltage of $V_{0\,\max}$. As shown in the current paper, with the growing number of arms of an RF electrode, the therapeutic areas of heat penetration may be

successfully increased, adapting the used multi-tine applicator to the size and shape of the tumor treated with RF ablation procedures.

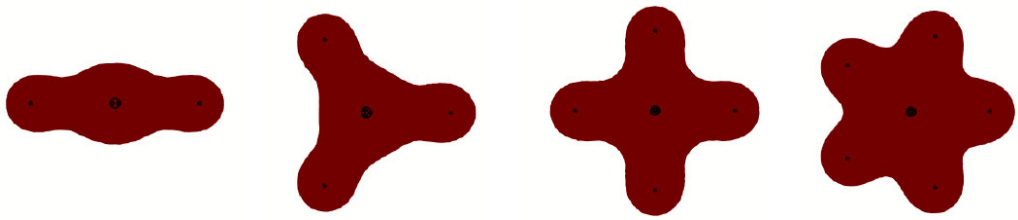

(a) (b) (c) (d)

Fig. 5. The isothermal contours for temperature 50°C in the xy-plane ($z = 0$) for analyzed cases: (a) 2-; (b) 3-; (c) 4-; (d) 5-tine electrodes during ablation procedures for $V_{0\,\max}$

Fig. 6 illustrates the Arrhenius damage index within treated tissue under ablative heating in 110°C in the case of the analyzed electrode with two arms. Since the Ω-parameter in the steady state conditions assumes a significant value of about $2.24 \cdot 10^7$, therefore the Arrhenius integral has been limited to 1 and 4.63. Importantly, these levels are respectively agreed to 63% and 99% probability of liver cell necrosis. Next charts indicate the transient dependences for the following parameters: Ω (Fig. 7(a)) and α (Fig. 7(b)) in a pre-defined control point and under various temperatures corresponding to different electrode voltages. As expected, the Arrhenius integral increases 'linearly' and the survival fraction decreases monotonically to zero over time.

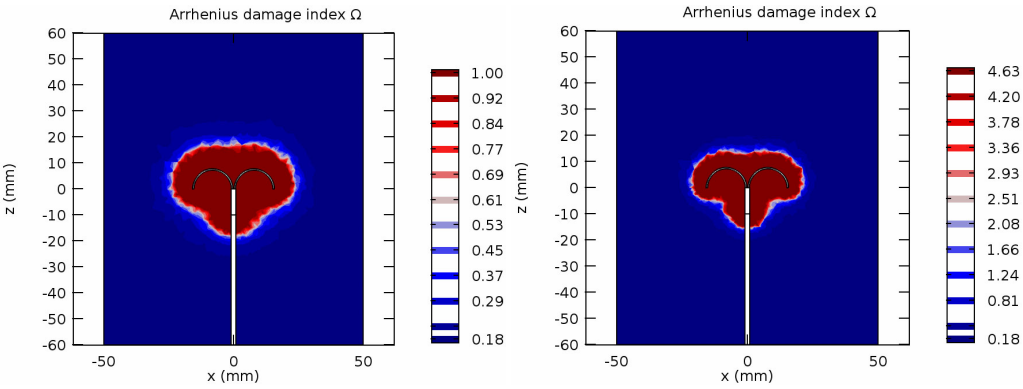

(a) (b)

Fig. 6. Examples of xz-distributions of the Arrhenius integrals limited to (a) Ω = 1 and (b) Ω = 4.63 derived from the 2-tine electrode inside liver tissue during ablation in the steady-state for $V_{0\,\max}$

Fig. 8(a) depicts the time transient distributions of necrotic fraction of hepatic tissue for example voltages applied to the 2-tine electrode. The initial zero state means that all hepatic cells are alive before thermal ablation. During the treatment the necrotic fraction increases. In the case of a voltage level of 9.40 V used, the θ-parameter reaches a steady-state after approximately 8 minutes, while for $V_0 = 22.28$ V the same parameter achieves a value of 1 after just 25 seconds,

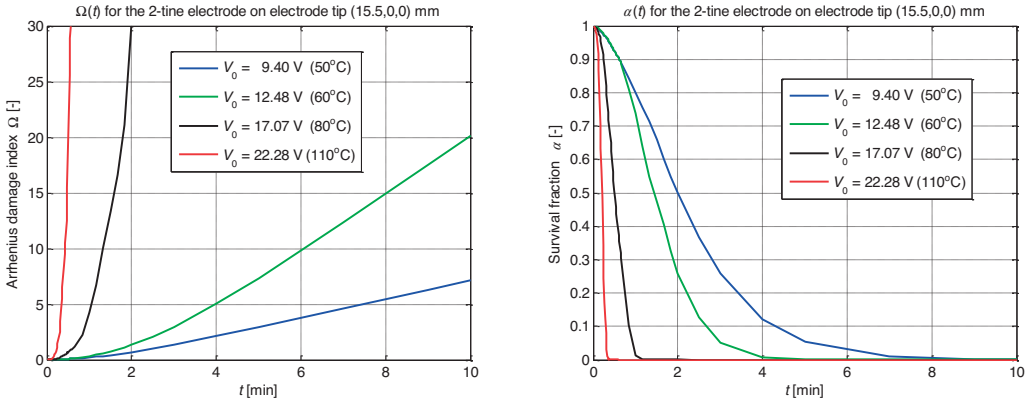

(a) (b)

Fig. 7. Time dependences of: (a) Arrhenius damage index and (b) survival fraction of liver tissue for different values of electrode voltage on tip of the 2-tine electrode

i.e. the state, where all liver cells are irreparably damaged. The necrosis of living hepatic cells at a similar time period is observed for multiple armed RF applicators in the case of ablative heating at 110°C (see Fig. 8b).

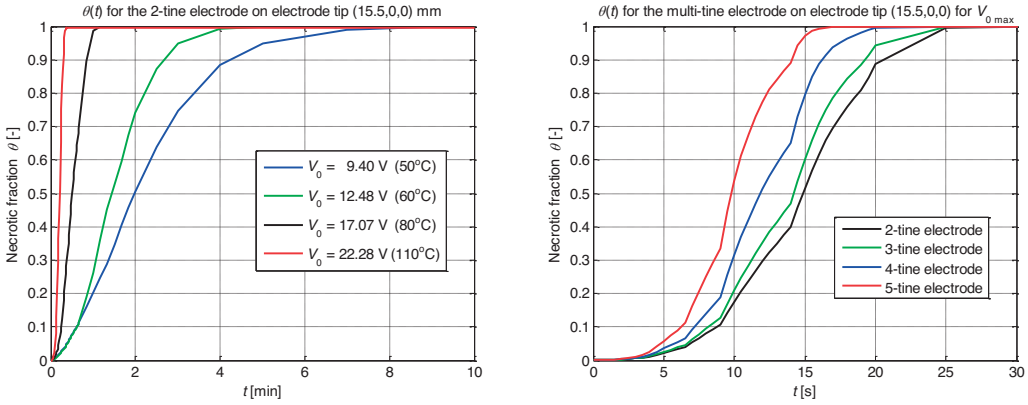

(a) (b)

Fig. 8. Time dependences of necrotic fraction of human liver tissue for: (a) different values of electrode voltage on tip of the 2-tine electrode and for (b) analyzed multi-tine electrodes during ablation procedures for $V_{0\,\max}$

4. Conclusions

Radiofrequency ablation (RFA) has been used for many years with proven efficiency in treatment of soft tissue, as well as liver, lung, kidney and bone cancers. Thermal changes in human tissues could be modelled numerically with the finite element method. In this paper the

impact of multi-tine electrode configuration in a realistic 3D model of RF ablative heating has been examined. As shown above, the therapeutic response of hepatic cells during an RFA procedure depends on many factors, including the geometry of an electric probe, applied electrode voltage, electro-thermal properties of an applicator and surrounding liver tissue, as well as duration of the treatment.

It was clearly demonstrated that a growing number of equally spaced arms within the multi-tine electrode requires increasing voltage values on an RF electrode surface to induce the same therapeutic effects. Moreover, by choosing the proper electrode configuration, we can influence the size and shape of ablative lesions inside the treated tissue, and thereby adjust the applicator type into the hepatic tumor of a particular patient. Of course, the employed electrode voltage (temperature) directly affects the necrosis of hepatic cells.

In the case of ablative heating at 110°C derived from the 2-tines electrode, the necrotic fraction of liver cells reaches its maximum value just after 25 seconds. What is more interesting, at a temperature of 50°C, the same tissue state, where all cells are irreparably damaged, occurs after 8 minutes. Similar hepatic cell behavior can be observed for other multi-tine electrodes.

The presented considerations may have enormous significance in the practical implementation of real-time RF ablation treatment of hepatocellular carcinoma.

References

[1] Vogl T.J., Nour-Eldin N.A., Hammerstingl R.M., Panahi B., Naguib N.N.N., *Microwave Ablation (MWA): Basics, Technique and Results in Primary and Metastatic Liver Neoplasms–Review Article*, RoFo – Fortschritte auf dem Gebiet der Rontgenstrahlen und der Bildgebenden Verfahren, vol. 189, no. 11, pp. 1055–1066 (2017).

[2] Tungjitkusolmun S., Staelin S.T., Haemmerich D., Jang-Zern Tsai, Hong Cao, Webster J.G., Lee F.T., Mahvi D.M., Vorperian V.R., *Three-dimensional finite-element analyses for radio-frequency hepatic tumor ablation*, IEEE Transactions on Biomedical Engineering, vol. 49, no. 1, pp. 3–9 (2002).

[3] Cala P., Bienkowski P., *The concept and design of an interstitial microwave hyperthermia antenna with directional radiation characteristics*, Przeglad Elektrotechniczny, vol. 94, no. 1, pp. 9–12 (2018).

[4] Al-Alem I., Pillai K., Akhter J., Chua T.C., Morris D.L., *Heat sink phenomenon of bipolar and monopolar radiofrequency ablation observed using polypropylene tubes for vessel simulation*, Surgical Innovation, vol. 21, pp. 269–276 (2014).

[5] Gas P., Kurgan E., *Evaluation of thermal damage of hepatic tissue during thermotherapy based on the Arrhenius model*, 2018 Progress in Applied Electrical Engineering (PAEE), IEEE Xplore, pp. 1–4 (2018), DOI: 10.1109/PAEE.2018.8441065.

[6] Antunes C.L., Almeida T., Raposeiro N., *Producing a Regular Thermal Lesion Volume on a Cholangiocarcinoma Considering a Saline-Enhanced RF Ablation*, Przeglad Elektrotechniczny, vol. 88, no. 7b, pp. 24–27 (2012).

[7] Paruch M., Turchan Ł., *Mathematical modelling of the destruction degree of cancer under the influence of a RF hyperthermia*, AIP Conference Proceedings, vol. 1922, no. 1, art. 060003, pp. 1–10 (2018), DOI: 10.1063/1.5019064.

[8] Gas P., Miaskowski A., *SAR optimization for multi-dipole antenna array with regard to local hyperthermia*, Przeglad Elektrotechniczny, vol. 95, no. 1, pp. 17–20 (2019), DOI: 10.15199/48.2019.01.05.

[9] Ge M., Jiang H., Huang X., Zhou Y., Zhi D., Zhao G., Chen Y., Wang L., Qiu B., *A multi-slot coaxial microwave antenna for liver tumor ablation*, Physics in Medicine and Biology, vol. 63, no. 17, art. 175011, pp. 1–13 (2018).

[10] Voglreiter P., Panchatcharam Mariappan, Pollari M., Flanagan R., Sequeiros R.B., Portugaller R.H., Fütterer J., Schmalstieg D., Kolesnik K., Moche M., *RFA Guardian: Comprehensive Simulation of Radiofrequency Ablation Treatment of Liver Tumors*, Scientific Reports, vol. 8, no. 787, pp. 1–13 (2018).

[11] Wang Z., Aarya I., Gueorguieva M., Liu D., Luo H., Manfredi L., Cuschieri A., *Image-based 3D modeling and validation of radiofrequency interstitial tumor ablation using a tissue-mimicking breast phantom*, International Journal of Computer Assisted Radiology and Surgery, vol. 7, no. 6, pp. 941–948 (2012).

[12] Singh S., Repaka R., *Numerical study to establish relationship between coagulation volume and target tip temperature during temperature-controlled radiofrequency ablation*, Electromagnetic Biology and Medicine, vol. 37, vol. 1, pp. 13–22 (2018).

[13] Audigier C., Mansi T., Delingette H., Rapaka S., Passerini T., Mihalef V., Pop R., Diana M., Soler L., Kamen A., Comaniciu D., Ayach N., *Challenges to validate multi-physics model of liver tumor radiofrequency ablation from pre-clinical data*, Computational Biomechanics for Medicine, pp. 2–38 (2016).

[14] Soetaert F., Crevecoeur G., Dupre L., *Coupled electrical-thermal model for monopolar and bipolar radiofrequency liver tumor ablation*, 2016 International Symposium on Fundamentals of Electrical Engineering (ISFEE), IEEE Xplore, pp. 1–5 (2016).

[15] Zhao Wei, Zhao-Hong Peng, Jin-Zhou Chen, Ji-Hong Hu, Jian-Qiang Huang, Yong-Neng Jiang, Gang Luo, Gen-Fa Yi, Hui Wang, Shen Jin, Bu-Lang Gao, *Thermal effect of percutaneous radiofrequency ablation with a clustered electrode for vertebral tumors: In vitro and vivo experiments and clinical application*, Journal of Bone Oncology, vol. 12, pp. 69–77 (2018).

[16] Frank K., Lindenborn H., Dahlhaus D., *Numerical and experimental characterization of radiofrequency ablation in perfused kidneys*, 2012 Annual International Conference of the IEEE Engineering in Medicine and Biology Society (EMBC), pp. 5707–5711 (2012).

[17] Hanks B., Frecker M., Moyer M., *Optimization of a Compliant Endoscopic Radiofrequency Ablation Electrode*, ASME 2017 International Design Engineering Technical Conferences and Computers and Information in Engineering Conference, vol. 5A, no. DETC2017-67357, pp. 1–12 (2017).

[18] Mellal I., Kengne E., El Guemhioui K., Lakhssassi A., *3D modeling using the finite element method for directional removal of a cancerous tumor*, Journal of Biomedical Sciences, vol. 5, no. 4, no. 28, pp. 1–8 (2016).

[19] Pop M., Davidson S.R.H., Gertner M., Jewett M.A.S., Sherar M.D, Kolios M.C., *A Theoretical Model for RF Ablation of Kidney Tissue and Its Experimental Validation*, Lecture Notes in Computer Science, vol. 5958, pp. 119–129 (2010).

[20] Ali M.T. *et al.*, *Malignant kidney tumor ablation using electric probe heating*, 2016 International Workshop on Computational Intelligence (IWCI), pp. 106–109 (2016).

[21] Chaichanyut M., Tungjitkusolmun S., *Microwave Ablation Using Four-Tine Antenna: Effects of Blood Flow Velocity, Vessel Location, and Total Displacement on Porous Hepatic Cancer Tissue*, Computational and Mathematical Methods in Medicine, vol. 2016, no. 4846738 (2016).

[22] Duan Bin, Wen Rong, Fu Yabo, Chua Kian-Jon, Chui Chee-Kong, *Probabilistic finite element method for large tumor radiofrequency ablation simulation and planning*, Medical Engineering and Physics, vol. 38, no. 11, pp. 1360–1368 (2016).

[23] Corral-Bustamante R.L., Trevizo M.A.F., Hernandez-Magdaleno J.N., *Modeling of Shape Memory Alloys for Medical Design in Robotics*, Manufacturing Science and Technology, vol. 3, no. 4, pp. 82–97 (2015).

[24] Kosturski N., Margenov S., Vutov Y., *Comparison of Two Techniques for Radio-frequency Hepatic Tumor Ablation through Numerical Simulation*, AIP Conference Proceedings, vol. 1404, no. 1, pp. 431–437 (2011).

[25] Chang I.A., *Considerations for thermal injury analysis for RF ablation devices*, The Open Biomedical Engineering Journal, vol. 4, pp. 3–12 (2010).

[26] Ulucakli M.E., *Radiofrequency Catheter Ablation of Cardiac Arrhythmias*, ASME 2011 International Mechanical Engineering Congress and Exposition, pp. 335–350 (2011).

[27] Chen Q., Müftü S., Meral F.C., Tuncali K., Akçakaya M., *Model-based optimal planning of hepatic radiofrequency ablation*, Mathematical Medicine and Viology: A Journal of the IMA, vol. 34, no. 3, pp. 415–431 (2017).

[28] Pennes H.H., *Analysis of Tissue and Arterial Blood Temperatures in the Resting Human Forearm*, Journal of Applied Physiology, vol. 85, no. 1, pp. 5–34 (1998).

[29] Soetaert F., *Experimental and Numerical Analysis of Magnetic Nanoparticle Hyperthermia: an Interdisciplinary Cancer Treatment*, PhD Thesis, Ghent University (2017).

[30] Wright N.T., *Quantitative Models of Thermal Damage to Cells and Tissues*, Heat Transfer and Fluid Flow in Biological Processes, pp. 59–76 (2015).